# CMOS AVALANCHE ELECTROLUMINESCENCE APPLICATIONS – MICRODISPLAY AND HIGH SPEED DATA COMMUNICATION

**M.E. Goosen*, M. du Plessis**, P.J. Venter**, A.W. Bogalecki*, A.C. Alberts* and P. Rademeyer**

** INSiAVA (Pty) Ltd, P.O. Box 14679, Hatfield, 0028, Pretoria, South Africa*
*E-mail: marius.goosen@up.ac.za*
*** Carl and Emily Fuchs Institute for Microelectronics, Dept. of Electrical, Electronic & Computer Engineering, Corner of University Road and Lynnwood Road, University of Pretoria, Pretoria 0002, South Africa*

**Abstract:** All-CMOS silicon light sources, although not the choice semiconductor process for light generation, offer the possibility of large scale manufacturing, integration with digital and driver electronics as well as a wide operating temperature range. These advantages do however come at a cost of reduced efficiency, but offer significant cost advantages inherent when using a standard CMOS technology. This paper presents two applications of standard CMOS integrated light sources. A fully functional microdisplay utilising avalanche electroluminescence for visible light generation and implemented in a completely standard 0.35 µm CMOS technology is presented. The microdisplay has an operating temperature range of -50 to 125 °C, which cannot be achieved by competing microdisplay technologies. Utilising the same silicon light sources, a 10 Mb/s optical communication link is established operating at a BER of less than $10^{-12}$. The data communication link presented in this paper constitutes the fastest all-silicon data communication link achieved thus far.

**Key words:** Microdisplay, Optical interconnect, silicon light emission, silicon photonics

## 1. INTRODUCTION

Avalanche electroluminescence in the visible spectrum from *pn*-junctions was reported for the first time in 1955 [1]. Due to the low internal quantum efficiency of indirect bandgap silicon light emitters, the main industry approach was to use III-V element as well as organic material emitters to accomplish light emission for applications ranging from long-haul optical communication links to microdisplays.

In a microdisplay market dominated by OLED and LCD technologies, a fully integrated CMOS microdisplay, fabricated in the 0.35 µm *austriamicrosystems* (AMS) CMOS process with no process modifications or post-processing, has a number of attractive advantages which could be exploited to lead to interesting applications in this environment. The advantages include the use of a robust and mature technology which is CMOS, resulting in favourable cost, configurability, wide operating temperature range and reliability. The reliability of silicon light sources has been shown through accelerated stress tests resulting in negligible intensity variations under all conditions of aging [2]. Other silicon-based microdisplays, implemented using porous silicon, were deemed quite promising for near-the-eye (NTE) applications where low luminance levels are sufficient for direct viewing [3, 4].

Short distance communication, such as chip-chip, board-board and rack-rack interconnects, require less optical power to maintain an acceptable BER. Hence low efficiency silicon light emitters become a viable solution, although at a cost of higher power dissipation [5]. The low efficiency of the indirect bandgap silicon light emitters, if optimised, can be utilised in high speed all-silicon optical interconnects [6, 7].

Section 2 describes the silicon light emitters utilised for both the all-CMOS microdisplay as well as the high speed data optical transmission presented in Section 3 and Section 4 respectively.

## 2. SILICON LIGHT EMITTERS

The silicon light emitters utilised in this research are formed in bulk silicon with the creation of reverse biased *pn*-junctions. The reverse biased *pn*-junctions, operated in the avalanche breakdown region, are shaped to form a point, hence aptly named point sources, in order to enhance the local current density and increase the external power efficiency (EPE).

Light directing structures utilising the back-end-of-line (BEOL) stack direct the light generated in the bulk toward the $SiO_2$-air interface improving the light extraction efficiency (LEE) by an average factor of 2.18 [8]. The BEOL-stack reflectors can be designed to either focus the light into a narrow pencil-beam for coupling into an orthogonally aligned optical fibre for communication or to generate a wide beam width for a microdisplay with a wider half-power viewing angle. Additional techniques to further increase the light extraction efficiency of punch-through and reach-through devices have also been demonstrated [9], indicating the

possibility of increased optical output power and higher data rates.

The emission spectrum, ranging from 400 nm up to 1000 nm allows for both viewing applications, such as a microdisplay, and short-distance optical communication. Figure 1 illustrates the emission spectrum of a silicon light emitter. The photopic luminance function is also shown as indication of the typical spectrum that the human eye perceives under well-lit conditions.

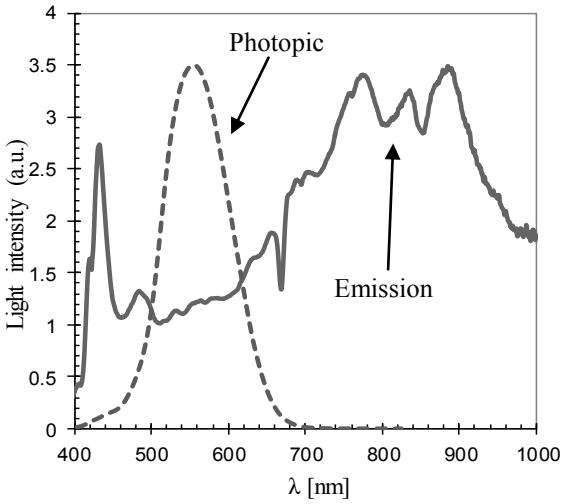


Figure 1. Emission spectrum of the silicon light source driven under avalanche conditions as well as the photopic luminosity function.

The photopic luminosity function as shown in Figure 1, is relatively narrow compared to the emission spectrum of the silicon light source. Approximately 10 % of the emitted optical power falls in the photopic region seen by the eye. For optical data communication, the majority of the spectrum is covered by commercially available silicon avalanche photodiodes (APDs), usually with peak responsivity at around 800 nm.

## 3. ALL-CMOS MICRODISPLAY

### *3.1 Microdisplay design*

Each pixel within the 8x64 pixel dot-matrix display is comprised of 30 individual point sources, each with their own BEOL reflector. The minimum pixel dimension is hence determined by the BEOL reflector aperture, which is approximately 5 µm. Each 50 µm pixel was connected to a row-select line as well as a column-select line. The column-select lines were combined into a 6-64 decoder to reduce the amount of interface interconnects. Figure 2 illustrates the scanning methodology utilised in the microdisplay.

A column is activated through the applied 6-bit word (only one column active at any given moment), and any of the individually addressed rows can be activated, activating and driving the chosen pixel. For sequential scanning, the active column will move one column right or left, and the rows are used to choose the active pixels. This process continues, allowing flicker-free image formation.

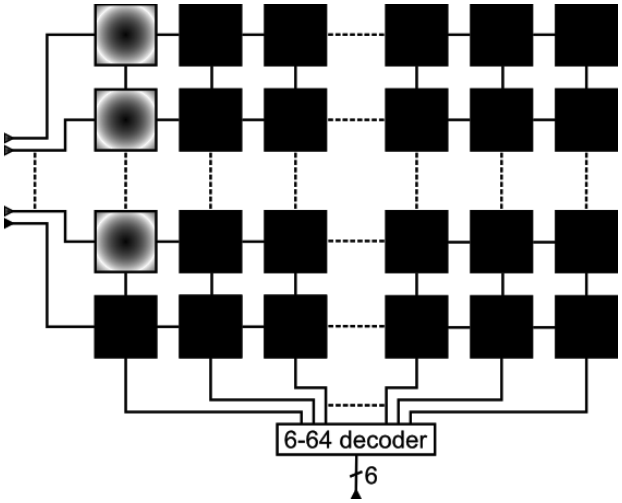


Figure 2: Illustration of the scanning methodology employed for image formation.

The half power viewing angle of the display is dependent on the type of BEOL reflector implemented on each of the point sources within the pixel. Figure 3 illustrates the 3D radiation pattern of the microdisplay.

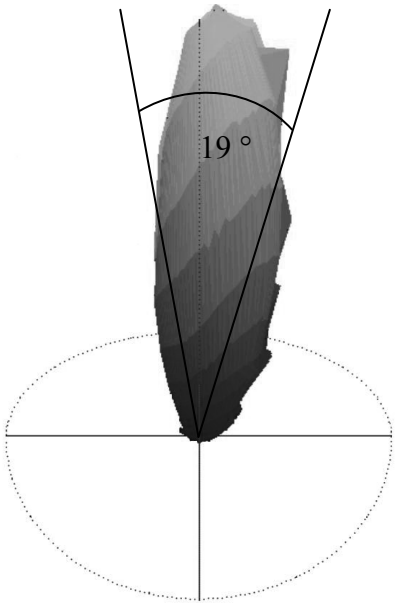


Figure 3. 3D radiation pattern of the implemented microdisplay. The measured half power viewing angle is 19 degrees.

### *3.2 Results*

As indicated in Figure 3, a half power viewing angle of 19 degrees was achieved, although it should be noted that the viewing angle is determined by the variable BEOL reflector. The half power angle was measured using a photomultiplier tube (PMT) with a small circular aperture, in conjunction with a goniometer, rotating the

microdisplay in fixed steps over the two spherical axes around the PMT. A viewing angle of 19 degrees is ample for NTE applications where the display is held in a fixed position relative to the eye. It can also be noted that the radiation pattern is slightly slanted due to the general direction to which the planar light sources are aligned.

The prototype developed depends on external control for the rendering of characters and images. Grey scale images can be produced by either using pulse width modulation (PWM) or current controlled pixels. Since the microdisplay is formed using the emissive silicon light sources, a true black can be achieved with an inactive pixel.

Figure 4 illustrates an image formed on the all-CMOS microdisplay, followed by a grey scale bar implemented with the use of PWM.

Figure 4: Image formed on the all-CMOS microdisplay clearly showing the illuminated pixels in contrast to the true-black (off) pixels [10].

The image as shown in Figure 4 was formed without the use of an image intensifier. The CMOS display as shown has sufficient optical power in the photopic region for direct viewing with a simple magnification lens.

## 4. HIGH SPEED DATA TRANSMISSION

### *4.1 Communication link setup*

Figure 5 illustrates the optical communication link setup used in the data rate demonstration.

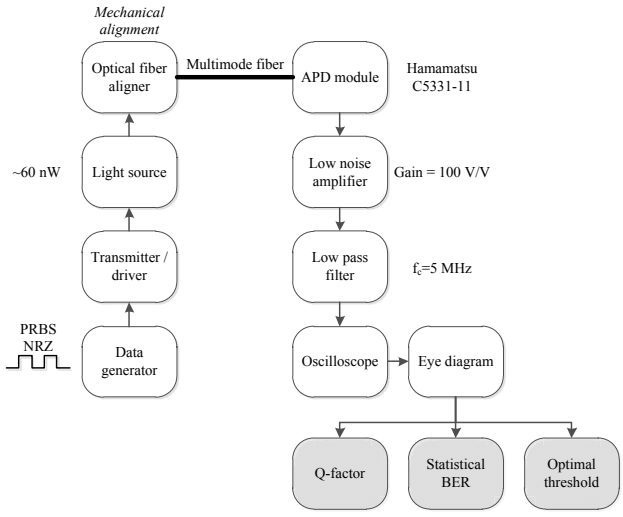


Figure 5: High speed optical communication setup.

A data generator was used in the creation of pseudo-random NRZ sequences and applied to the transmitter/ driver. The transmitter/ driver implemented a differential driving scheme in order to reduce electromagnetic radiation due to large switching currents. One of the directly modulated light sources, capable of delivering up to 60 $nW_{peak}$ of optical power, was mechanically aligned with a low attenuation step index multimode fibre (MMF) with a core-diameter of 600 µm. The light source array was matched to the core diameter of the fibre, resulting in a total of 3520 point sources. The light source array was biased and driven for maximum extinction ratio to maximise the achieved signal to noise ratio (SNR). The MMF exhibits a low attenuation in the region spanning from 400 nm up to 2000 nm, hence in the silicon emission spectrum.

A commercial APD, *Hamamatsu 5331-11*, was used to convert back to the electrical domain before amplification and filtering. The APD has an active area diameter of 1 mm, hence no lenses are required to couple from the fibre to the photodiode. It further has a peak responsivity at 620 nm of 0.42, a transimpedance gain of 40 kΩ and a noise density referred to the input of approximately 0.5-1 pW/√Hz.

The low noise amplifier was implemented using 2 stages, each with a 10 V/V gain, and a total noise density of 20 nV/√Hz. The filter cut-off frequency was chosen as half the data rate, hence 5 MHz, suppressing additional frequency components introducing inter-symbol interference.

### *4.2 Results*

An oscilloscope was used, as recommended by ITU-T G.976 [11] and discussed in [7], in order calculate a quality factor (Q-factor) which relates the signal power to the noise power, hence a statistical SNR, within the eye diagram. From the calculated Q-factor the statistical BER and optimal sampling threshold is determined. The eye diagram achieved after filtering is depicted in Figure 6.

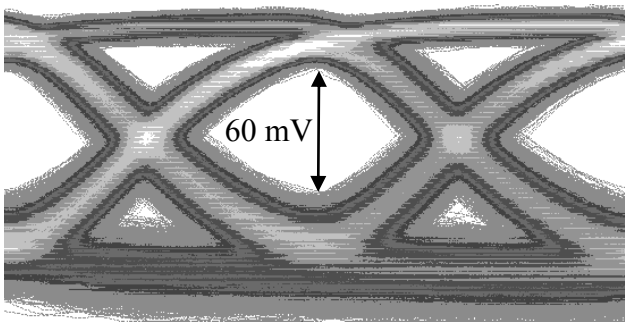


Figure 6: Eye diagram of the high speed optical communication link at a data rate of 10 Mb/s.

The increased amount of noise in the lower level of the eye diagram in Figure 6 is due to the increased amount of shot noise generation with a larger incoming optical signal. The APD utilised has an inverting gain

transimpedance amplifier, hence the low level in the eye diagram is in fact the high level of the optical signal. The statisctical information extracted from the eye diagram is depicted in Figure 7.

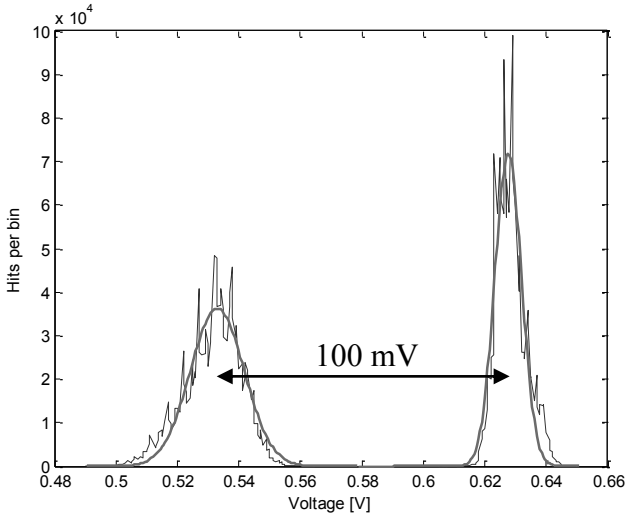


Figure 7. Histogram of the vertical eye opening.

The noise in the vertical eye amplitude follow a Gaussian distribution since there are no channel bandwidth limitations closing the eye in a deterministic fashion. Hence, a Gaussian distribution was fitted to the noise in order to optain the noise in the eye as is shown in Figure 7.

The eye diagram in conjunction with the statistical information gathered by the histogram, results in a calculated Q-factor of 7.22, an optimal sampling threshold of 0.59 V and a statistical BER of $2.64 \times 10^{-13}$. The achieved SNR for the 10 Mb/s optical data communication link equates to 26.05. It is noted that the data rate achieved is not limited by the switching capability of the silicon light sources, but rather by the achievable optical output power and the noise contribution of the APD determining the SNR and BER. Silicon light sources have been shown to switch in excess of 350 MHz, through E-O-E testing [7], and in excess of 20 GHz using streak camera techniques for emission resulting from hot carrier luminescence [12].

Another fact worth mentioning is the low LEE which is currently achieved. The LEE is defined as the percentage of light which can be directed to exit the surface. Currently, only about 1 % of the generated optical power exits the surface of the die, of which another 10 % is lost due to the fibre coupling efficiency. Hence, taking these factors into account approximately 6.6 µW is generated on the CMOS die.

The previous fastest reported all-CMOS optical communication link achieved a data transfer rate of 1 Mb/s at a BER of $10^{-14}$ [7]. In order to achieve a data transfer rate of 10 Mb/s the amount of input optical power has to scale with the square root of the bandwidth increase. Hence, a factor 3.3 improvement is necessary for scaling from 1 Mb/s to 10 Mb/s. The BER curves at the different data rates are illustrated in Figure 8. The demonstrated data transfer rates are indicated by encircled points.

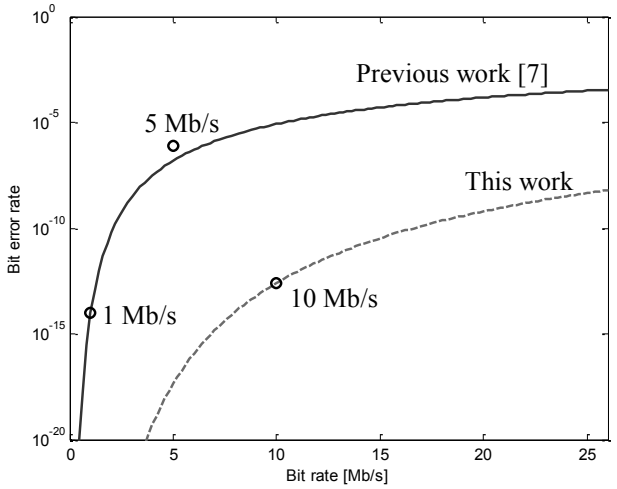


Figure 8. Theoretical BER versus bit rate curves. Solid line – results presented in [7]. Dashed line – result presented in this paper.

## 5. CONCLUSION

The electrical performance parameters of the prototype all-CMOS microdisplay is presented in Table 1.

Table 1. CMOS dot matrix display electrical characteristics

| Parameter | Typical | Units |
|---|---|---|
| Si source breakdown voltage | 9.2 | V |
| Supply voltage | 12 | V |
| Current per pixel | 5.1 | mA |
| Maximum current (all pixels on) | 41 | mA |
| Power consumption (all pixels on) | 0.492 | W |
| Refresh rate | 42.8 | Hz |
| Pixel pitch | 50 | µm |
| Display active area | 1.32 | $mm^2$ |
| Half power viewing angle | 19 | ° |

The cost benefit and flexibility coupled with the robustness of the mature technology which is CMOS, may lead to interesting applications in the microdisplay environment. One interesting possibility is the combination of an optical communication link and a microdisplay, since the silicon light sources are inherently fast switching devices [13]. With an increase in device efficiency, the power consumption can be reduced while maintaining the same luminance. Although not comparable to OLED and LCD technologies in terms of power consumption and resolution, the wide operating temperature range and implementation flexibility should allow all-CMOS microdisplays to be applied in certain niche markets.

An all-silicon optical communication link was demonstrated operating at a data transfer rate of 10 Mb/s

while maintaining a statistical BER of less than $10^{-12}$, a tenfold increase in data transfer rates over previous reported all-silicon communication links [7]. The light sources were implemented in standard 0.35 μm CMOS process, with no post-processing, obtaining results exceeding other more exotic silicon-based technologies [5]. With increased EPE and LEE of the silicon light emitters, multi-Gb/s optical interconnects for short-haul communications remain feasible and attractive.

## 6. ACKNOWLEDGMENTS

The authors would like to thank INSiAVA (Pty) Ltd (http://www.insiava.com) for funding this research.

## 7. REFERENCES

[1] R. Newman, "Visible light from a silicon p-n junction", Phys. Rev., 100(2), pp. 700–703, 1955.

[2] A. Chatterjee and B. Bhuva, "Accelerated Stressing and Degradation Mechanisms for Si-Based Photoemitters", IEEE Trans. on Device and Materials Reliability, 2(3), pp. 60-64, 2002.

[3] A. Smirnov, A. Berezovik, P. Poznyak, V. Labunov, S. Lazarouk, "Silicon based LED microdisplays: The experience of design and manufacturing," Proc. of SPIE Vol. 6637, XV International Symposium on Advanced Display Technologies, 663703, 2007.

[4] P. Jaguiro, P. Katsuba, S. Lazarouk, M. Farmer, A. Smirnov, "Si-based emissive microdisplays," Physica E 41, pp. 927–930, 2009.

[5] S. Sayil, "Avalanche breakdown in silicon devices for contactless logic testing and optical interconnect", Analog Integrated Circuits and Signal Processing, 56(3), pp. 213-221, 2008.

[6] M. du Plessis, H. Aharoni and L.W. Snyman, "Silicon LEDs fabricated in standard VLSI technology as components for all silicon monolithic integrated optoelectronic systems", IEEE Journal on selected topics in Quantum Electronics, 8(6), pp. 1412-1419, 2002.

[7] M.E. Goosen, P.J. Venter, M. du Plessis, I.J. Nell, A.W. Bogalecki and P. Rademeyer, "High-speed CMOS optical communication using silicon light emitters", Paper 7944-32, Session 9, Proc. SPIE 7942, SPIE Photonics West, San Francisco, USA, 26 January 2011.

[8] A.W. Bogalecki, M. du Plessis, P.J. Venter, M.E. Goosen and I.J. Nell, "Integrated optical light directing structures in CMOS to improve light extraction efficiency", Proc. of the International Conference on Microelectronics, Cairo, pp. 168-171, 19-22 Dec. 2011.

[9] P.J. Venter, M. du Plessis, I.J. Nell, A.W. Bogalecki, and M.E. Goosen, "Improved efficiency of CMOS light emitters in punch through with field oxide manipulation", Proc. of the International Conference on Microelectronics, Cairo, pp. 36-39, 19-22 Dec. 2011.

[10] P.J. Venter, A.W. Bogalecki, M. du Plessis, M.E. Goosen and I.J. Nell, "CMOS dot matrix microdisplay", Proceedings of the Advances in Display Technologies conference, Proc. SPIE 7956, Paper 79560Y; SPIE Photonics West, San Francisco, California, USA, 22-27 January 2011.

[11] ITU-T Recommendation G.976, "Digital transmission systems – Digital sections and digital line system – Optical fibre submarine cable systems", Series G: Transmission Systems and Media, Digital Systems and Networks, 1997.

[12] A. Chatterjee, B. Bhuva and R. Schrimpf, "High speed light modulation in avalanche breakdown mode for Si diodes", IEEE Electron Device Letters, 25(9), pp. 628-630, 2004.

[13] J.J.D. McKendry, R.P. Green, A.E. Kelly, Z. Gong, B.G.D. Massoubre, E. Gu, M.D. Dawson, "High-speed visible light communications using individual pixels in a micro light-emitting diode array", IEEE Photonics Technology Letters, 22(18), 2010.